A&A 511, A70 (2010)
DOI: 10.1051/0004-6361/200912516

Astronomy & Astrophysics

A detailed study of the main sequence of the globular cluster NGC 6397: can we derive constraints on the existence of multiple populations?

M. Di Criscienzo, F. D'Antona, and P. Ventura

Osservatorio Astronomico di Roma, via di Frascati 33, 00040, Monte Porzio Catone, Rome, Italy
e-mail: [dicrisci;dantona;ventura]@oa-roma.inaf.it

Received 18 May 2009 / Accepted 15 December 2009

ABSTRACT

Context. Globular clusters can no longer be regarded as examples of "simple stellar populations" as all those so far examined contain an important fraction of "second generation" stars, in which the light elements are processed through the hot CNO cycle, and helium variations may be present. Clusters apparently "simple" contain a majority of second generation stars.
Aims. If NGC 6397 contains a large fraction of "second generation" stars (>70% according to recent analysis), the helium abundance of its stars might also be affected, show some star-to-star variation, and be larger than the standard Big Bang abundance $Y \sim 0.24$. Can we derive constraints on this issue from the analysis of the main sequence width and from its luminosity function?
Methods. We build up new models for the turnoff masses and the main sequence down to the hydrogen burning minimum mass, adopting two versions of an updated equation of state (EOS) including the OPAL EOS. Models consider different initial helium and CNO abundances to cover the range of possible variations between the first and second generation stars. We compare the models with the observational main sequence. We also make simulations of the theoretical luminosity function, for different choices of the mass function and of the mixture of first and second generation stars and compare them with the observed luminosity function by means of the Kolmogorov Smirnov – KS-test.
Results. The new models for very low mass stars compare well with previous models and show that the OPAL EOS is a good description in all the region of temperature and densities of very low mass stars for which it is computable. The analysis of the main sequence width shows that any helium variation must be confined within $\Delta Y \sim 0.02$ in the case of a CNO increase as suggested by literature, and we discuss the consequent implications for the model of self-enrichment. We also show that the KS test on the luminosity functions allows us to derive a best distance modulus for each age. For a population all made by stars with standard helium $Y = 0.24$, standard CNO abundances, and an age of 12 Gyr, choosing a double power law mass function $\propto M^{-0.7}$ for $M > 0.18\ M_{\odot}$ and $\propto M^{-0.9}$ for $M < 0.18\ M_{\odot}$, the resulting theoretical luminosity function agrees well with the observed one (KS ~ 0.75 for a distance modulus $(m-M)_{F814W} = 12.31 \pm 0.05$ mag). Using non-standard CNO abundance for all the stars or for a fraction of 70%, the KS test provides comparable agreement (~KS > 0.55) with the observed luminosity function.
Conclusions. The study of the width of the main sequence at a different interval of magnitude is consistent with the hypothesis that both generations are present in the cluster. If the CNO increase suggested by spectroscopic observation is taken into account the small helium spread of the main sequence in NGC 6397 implies a substantial helium uniformity ($\Delta Y \sim 0.02$) between first and second generation stars. The possible spread in helium doubles if an higher larger increase of CNO is considered. The luminosity function is in any case well consistent with the observed data.

Key words. stars: general – stars: evolution – stars: low-mass – Hertzsprung-Russell (HR) and C-M diagrams – brown dwarfs

1. Introduction

Our views about globular clusters (GCs) are dramatically changing in recent years, thanks to precise photometric investigations that revealed the presence of multiple main sequences or subgiant branches (e.g. Piotto et al. 2007; Milone et al. 2008) and the increasing amount of new spectroscopic data on GC stars. These data, in particular the spectra for about 2000 stars in 19 GCs recently obtained by the multiobject spectrograph FLAMES@VLT (Carretta et al. 2009a,b) have shown how the "chemical anomalies" among GC stars are indeed ubiquitous in all clusters and concern a large fraction (from 50 to 80%) of stars. The peculiar chemical abundances take the form of anticorrelations between O and Na, Al and Mg, and are present in stars of various evolutionary phases (both unevolved main sequence and evolved red giant branch stars) (Gratton et al. 2001; Ramírez & Cohen 2002; Carretta et al. 2004), which supports the idea that they are not due to an "in situ" deep mixing in the stars, but have been imprinted in the gas from which they formed, which was polluted by the winds lost by a previous first generation (FG) of stars: according to this hypothesis, we are now seeing a second generation (SG) of stars mixed with the FG. It is not finally settled what kind of stars produced the material that must have been processed by the hot CNO cycle and other proton capture reactions on light nuclei. The two most popular candidates are massive asymptotic giant branch (AGB) stars (e.g. Ventura et al. 2001), and possibly, for the extreme anomalies, super-AGBs (Pumo et al. 2008).Alternative possibilities are massive

stars which are either fastly rotating (e.g. Decressin et al. 2007), or in binaries undergoing non-conservative evolution (de Mink et al. 2009).

Carretta et al. (2009a) examine the famous Na-O anticorrelation and tentatively divide the stars of each cluster into three groups: the "primordial" stars with abundances of O and Na similar to those found in the halo stars; the "intermediate" stars, which have high Na and a somewhat depleted O; the "extreme" stars, which have high Na and a strongly depleted O. While only a few very massive clusters contain stars with extreme anomalies, all clusters show a population with "intermediate" chemistry. The problem of GC formation and early evolution is very complex, but it is easy to accept that a cluster contains two or multiple populations if it shows both chemical peculiarities as discussed above, and also photometric peculiarities: the GC NGC 2808 is a prototype of this class[1], as it shows three populations both in the main sequence (Piotto et al. 2007) and in its horizontal branch (HB) extended morphology (D'Antona & Caloi 2004). It is possible to reproduce these three populations by assuming that they differ in helium content (e.g. D'Antona & Caloi 2008). Furthermore, this cluster shows the Na-O anticorrelation in one of its most extreme forms, with stars reaching very low oxygen abundances. Carretta et al. (2006) even find a possible indirect hint of helium enhancement in the subgroup of oxygen-poor red giants that they examine. As theory expects that some helium enrichment accompanies the hot-CNO nucleosynthesis in both the proposed models (massive AGBs or massive stars), NGC 2808 represents in many respects the most classic example of well-understood multiple populations in GCs.

There are other cases, however, in which the presence of subpopulations is not as clear, and where it is not clear, in particular, whether the abundance anomalies (in some cases less prominent, but always present, according to Carretta et al. 2009a) are *always* accompanied by helium enrichment, nor how large this enrichment is. The cluster NGC 6397 especially has always been considered the perfect example of a "simple stellar population" (SSP) due to the "tightness" of its HR diagram, which includes a very compact blue HB. In recent years, spectacular data for the low main sequence of NGC 6397 have become available. By using the technique of proper motion cleaning, Richer et al. (2006) obtained a very tight main sequence and a very clean luminosity function down to the hydrogen burning minimum mass (HBMM) (Richer et al. 2008). We decided to use these data to quantify at which level we can accommodate helium variations in this cluster (and the possible associated CNO variations), by investigating whether the main sequence width and its luminosity function are compatible with a helium spread and/or with a non-standard helium content. At the same time, we took the opportunity of this comparison to compute and test new stellar models for the low main sequence. In these models, we employ and compare new equations of state (EOS) today available, and we test the available color-$T_{\rm eff}$ transformations.

The outline of the paper is the following. In Sect. 2 we describe in some detail the spectroscopic results concerning the cluster and what we expect concerning the multiple populations it should hide and which plausible helium and C+N+O variations are expected. We then summarize the photometric data by Richer et al. (2008). After having summarized the literature concerning the low mass main sequence models, in Sects. 3 and 4 we describe our code and the results of the computation of solar scaled models; in Sect. 5 we present α-enhanced models computed for the comparison with the data for the Globular Cluster NGC 6397. Both the comparison of the CMD and the luminosity function with theory are discussed in detail in Sect. 6 also in the hypothesis of multiple populations with different helium and possibly also C+N+O, content. In Sect. 7 we summarize our results and conclusions.

2. The case of NGC 6397: apparently a simple stellar population

Carretta et al. (2009a) find that at least 70% of the stars in the cluster NGC 6397 are "intermediate" according to their definition, although photometric studies show that all the evolutionary sequences in this cluster look like those of a prototype SSP: the main sequence is very tight (King et al. 1998; Richer et al. 2006), and the horizontal branch (HB) lacks the extreme HB and blue hook stars that are now regarded as the proof of the presence of a very helium-enriched population (D'Antona et al. 2002; D'Antona & Caloi 2004). The chemical anomalies of the Carretta et al. (2009a) analysis, however, do not come as a complete surprise, as many hints were already available in recent literature about the dubious simplicity of this cluster. First of all, already Bonifacio et al. (2002) had noticed the presence of nitrogen-rich stars that have a normal Lithium content (see also Pasquini et al. 2008), and Carretta et al. (2005) find that only three subgiants out of 14 stars are nitrogen-normal. These features lead us to suspect that the material from which these stars formed is CNO processed, as expected in the stars with low oxygen and high sodium. The possible helium enhancement is certainly not extreme, as are for instance small lithium variations among the turnoff stars (Lind et al. 2009; Korn et al. 2007; Pasquini et al. 2008). In the massive AGB model for the formation of the second generation, the lithium content of the AGB ejecta is not as extremely depleted as in the other models, but it is difficult to believe in a cosmic conspiracy producing exactly the same lithium of the FG, unless the AGB matter is very diluted with FG gas, so that both lithium and helium do not differ too much in the two generations.

A different, mostly theoretical approach led Caloi & D'Antona (2005) and then D'Antona & Caloi (2008) to provocatively propose that *all* the stars in the clusters which have entirely blue HBs are composed by SG stars. This idea is at the basis of a possible explanation of the peculiar difference between the GCs M 3 and M 13. The cluster M 3 has a complex HB, including many stars redder than the RR Lyrae (a red clump), RR Lyrae stars, and a well populated blue side, while M 13, having the same metallicity, has an only-blue HB. This difference, which was generally attributed to different age (Johnson & Bolte 1998; Rey et al. 2001) or to different mass loss along the red giant branch (Lee et al. 1994; Catelan et al. 1998) (the famous second parameter problem) may also be interpreted by assuming that M 13 is totally deprived of its FG, and the SG has a minimum helium abundance with a mass fraction of $Y \sim 0.28$. In M 13, whose HB shows a prominent blue tail, simulations of the HB stellar distribution show that there must also be a small fraction of stars with helium $Y \sim 0.38$ (D'Antona & Caloi 2008). Is it possible that a GC is composed *only* of SG stars? This could indeed happen, as was shown in some hydrodynamic plus N-body simulations of the SG formation and of the cluster first phases of dynamical evolution presented by D'Ercole et al. (2008). They find that the dynamical evolution of the cluster may

[1] We do not wish to include ω Cen among the classic GCs, as it also shows large metallicity variations, indicating that its evolution is partially similar to that of a massive GC, containing e.g. a population with a very high helium content, but also closer to that of a small galaxy, as the supernova ejecta take part in the star formation events.

be characterized by an expansion of the FG star system due to the SNII mass loss preferentially occurring in the cluster central regions, while the SG is still forming in the core. Depending on the initial conditions, the ratio of SG to FG stars may in some cases even reach a factor of six or more. While this kind of modelling depends on the input parameters and does not imply that this really occurred in nature, NGC 6397, with its short blue HB, a tight main sequence (MS) and red giant branch (RGB) could indeed be made by a homogeneous set of SG stars, corresponding to a unique value of Y, just a larger than the Big Bang abundance ($Y \sim 0.26-0.28$). This speculation would help to understand why the nitrogen abundance in most of the NGC 6397 stars is quite large. The possibility that all the stars in this cluster have a homogeneous, but larger than standard, helium abundance could be falsified by looking at the main sequence width, which depends on the combination of the photometric errors with the possible star to star differences in helium.

Apart from this extreme and provocative suggestion, very recently Carretta et al. (2009a) show that only up to ~30% of stars should belong to the primordial population (the FG), under the assumption that all the stars within three sigma from the lowest sodium abundance measured in a cluster are "primordial"[2]. So at present the most reasonable assumption is that NGC 6397 has at least 70% of SG.

Given the sodium and oxygen abundances of the anomalous cluster stars, do we expect that they have an enhanced helium content? In the hypothesis that the SG is born from matter mixed with the hot-CNO processed ejecta of massive AGBs, we can look at the results by Ventura & D'Antona (2009). They interpret the anomalous Na-O abundances in NGC 6397 as a result of mixing between 50% of pristine gas with 50% of gas ejected by the 5 $M_{\odot}$ AGBs. Looking at Table 2 of their paper, the helium abundance in the 5 $M_{\odot}$ ejecta for $Z = 0.0006$ is $Y = 0.329$. A dilution by 50% with matter that has primordial $Y = 0.24$ provides indeed $Y = 0.285$. If we take these results at face value, the total CNO content of the SG stars is also higher than that of the FG stars. The 5 $M_{\odot}$ AGB evolution provides a CNO enhancement by a factor of about three, so we must also consider increased CNO (and total metallicity) by a factor of 1.5 when we compute the higher helium models. Of course, the computed AGB models do not give a mandatory prescription of what really happens in the cluster, so that we will also consider normal CNO models and models with even larger CNO to include all possible cases. Helium abundances equal to or larger than the standard ones will be considered up to $Y = 0.28$, to understand whether the hypothesis that at least ~70% of stars in NGC 6397 have an helium abundance larger than the Big Bang abundance is consistent with the photometric data.

2.1. The observational color–magnitude diagram of globular cluster NGC 6397

The first HST observations of the low MS of NGC 6397 date back to Paresce et al. (1995). Afterwards, King et al. (1998) have observed NGC 6397 with WFPC2@HST and found that the luminosity function has a rapid decline at low mass end. Recently, the most thorough observations by Richer et al. (2006, 2008) refined the data. They observed an outer region of NGC 6397 with ACS@HST using the photometric filters *F814W* and *F606W*. The high sensitivity of the camera, the large number of orbits obtained (=126) and the vicinity of the cluster (it is the second closest globular cluster, after M4) made it possible to reach the deepest intrinsic luminosities for a globular cluster achieved until today and what appears as the termination of the MS. The field observed overlaps that of archival WFPC2 data from 1994 and 1997, which were used for the proper-motion-cleaning of the data. This technique, applied to the deep ACS photometry, produces a very narrow MS till its end. These observations are a good basis to test the physics of low mass stars and the possible role of the helium abundance. Richer et al. (2008) analyzed the color−magnitude diagram (CMD) using the results of models computed with the Dartmouth Stellar Evolution Program (DSEP) (Dotter et al. 2007). Their main results are that

- the MS appears to terminate close to the CMD location of the HBMM predicted by models. The authors state that they would have found fainter MS stars in the cluster, if there had been any;
- the MS fitting technique provides a good agreement down to *F814W* = 22.5 mag; below this, down to ~24 mag, the isochrone is either too blue or too low in luminosity. The authors underline that this is likely due to low mass models being less luminous at a given mass than real stars;
- exploring the MS luminosity function, they find that a power law for the mass function MF well reproduces the distribution in luminosity of the observed stars, while a more top-heavy MF is necessary to fit the data in the cluster core that they also have available. However, theory predicts more stars than observed at the lowest MS luminosities, as also previously found by Montalban et al. (2000) using data by King et al. (1998).

3. The low mass main sequence models: input physics of the models

The computation of very low mass stellar models requires an accurate knowledge of the EOS for partially ionized gas at densities where the ideal gas EOS approximations breaks down dramatically, especially close to the pressure ionization region (Fontaine et al. 1977; Magni & Mazzitelli 1979; Saumon et al. 1995). The general properties of very low masses have been described in many works (for example see the reviews by Chabrier & Baraffe 1997; Alexander et al. 1997; Cassisi et al. 2000); for the population II low masses, after the work by D'Antona (1987), based on grey atmosphere boundary conditions and on the EOS by Magni & Mazzitelli (1979), Baraffe et al. (1997) presented models based on the Saumon et al. (1995) EOS and on the NextGen non-grey atmosphere models later on published by Hauschildt et al. (1999). They showed that this latter improvement was essential to reproduce the colors of the low mass main sequence. Montalban et al. (2000), reexamining the problem of the EOS, cautioned about the use of the additive volume interpolation needed to obtain the thermodynamic quantities for intermediate compositions from the pure hydrogen and pure helium tables available in the Saumon et al. (1995) EOS. In recent years, two new EOS have become available: the FreeEOS by Irwin (2004)[3] and the OPAL EOS, namely the EOS provided by the Livermore group as a byproduct of the opacity computation (Rogers et al. 1996). Both EOS do not cover the pressure ionization region however, for which the best approach remains that

[2] Indeed, while Carretta et al. (2009a) have only four "primordial" stars in their sample of O-Na measurements for this cluster, they have determined Na abundances in a larger number of stars, and also in this larger sample sodium is "normal", that is similar to the sodium of the halo stars that have a similar metallicity, in ~25−30% of stars.

[3] Technical Report http://freeeos.sourceforge.net/

by Saumon et al. (1995). The FreeEOS has been recently employed by Dotter et al. (2007) and applied to the fit of the main sequence of NGC 6397. The OPAL EOS has not yet been used to approach the construction of low mass models, so we decided to adopt it in two different ways in our new models, as described in Sect. 4.

We use the ATON code for stellar evolution; a detailed description can be found in Ventura et al. (2007); below we recall the main updated inputs that are important for the treatment of low mass stars.

3.1. Opacities and nuclear reaction

The program includes the opacities by Ferguson et al. (2005) for the external region of the star ($T \leq 15\,000$ K) and the latest version (2005) of OPAL opacities for higher temperatures (Iglesias & Rogers 1996). For fully convective low mass stars (below ~0.35 $M_\odot$) the uncertainties on radiative opacities have negligible influence on the models, while for larger masses an error in opacity by ~20% may cause an error up to ~1% in the determination of radii (Dotter 2007). Electron conduction opacities were taken from the WEB site of Potekhin (2006) and correspond to the Potekhin et al. (1999) treatment, corrected following the improvement of the treatment of the e−e scattering contribution described in Cassisi et al. (2007).

Although not necessary in this computation, the nuclear network includes 30 chemical elements, all main reactions of p−p, CNO, Ne-Na and Mg-Al chains and the α capture of all nuclei up ^{26}Mg. The relevant cross sections are from the NACRE compilation (Angulo et al. 1999).

3.2. Equation of state: OPAL vs. Saumon et al. (1995)

As remarked previously, non-ideal effects become increasingly important for masses $M \lesssim 0.8\ M_\odot$.

ATON uses 18 tables of EOS in the (gas)pressure-temperature plane corresponding to three different metallicities, $Z = 0$, 0.02 and 0.04, and six hydrogen mass fractions X, ranging from 0 to 1-Z; the thermodynamic quantities, i.e. density, adiabatic gradient, specific heat at constant pressure C_p, the C_p/C_v ratio, and the three exponents Γ_1, Γ_2 and Γ_3 are obtained via four cubic unidimensional splines on X, Z, pressure and temperature.

These 18 tables are constructed up in three steps. First, the thermodynamic quantities are computed according to the formulation by Stolzmann & Blöcker (2000), which is the most modern and updated description available for ionized gas, including both classic and relativistic degeneracy, coulombian effects and exchange interaction. The tables are then partially overwritten by the OPAL EOS in the whole domain where this is available (Rogers et al. 1996, see OPAL WEB page, last update in February 2006). Finally in the very low-temperature regime, where OPAL EOS is not available (see Fig. 1) the tables are overwritten by the Saumon et al. (1995) EOS, which has the advantage of employing an adequate physical model for the pressure ionization. The Saumon et al. EOS is only given for pure hydrogen and pure helium mixtures; the presence of metals is thus simulated by adding helium, and the different H-He mixtures must be interpolated through the additive volume law.

We call "EOS+OPAL" the tables that represent the standard in our computations. To investigate how the results depend on the chosen EOS, we built additional tables (EOS+SCH) using the EOS by Saumon et al. (1995, SCH) in the whole region of the $P - \rho$ plane for which it is available. This is an interesting test, because the structure of the majority of stars discussed here are contained in the region of plane $\mathrm{Log}\,T - \mathrm{Log}\,\rho$ where both EOS are available (see Fig. 1).

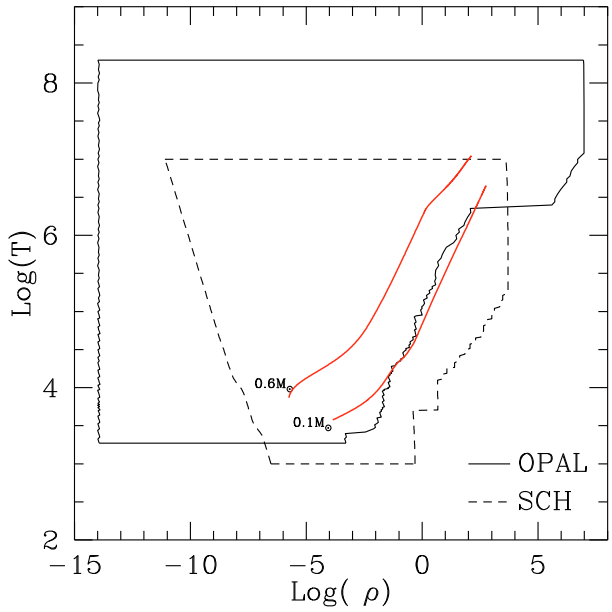

Fig. 1. We show the region of the Log(ρ) − Log(T) plane (density ρ in g cm^{-3} and temperature T in K) where OPAL (solid box) and SCH (dashed box) EOS are available. The structure profile of two stars with age = 10 Gyr, $Z = 0.0006$ and with $M = 0.6\ M_\odot$ and 0.1 $M_\odot$ are also shown. The 0.6 $M_\odot$ is in the region where the two EOS overlap, while 0.1 $M_\odot$ is exactly at the border between the two EOS.

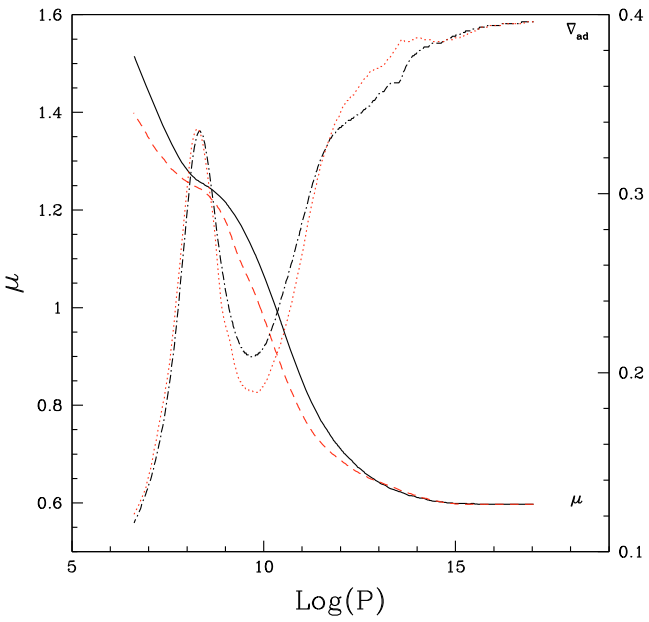

Fig. 2. Adiabatic gradient ($\nabla_{\rm ad}$; dash-dotted and dotted curves; right y-axis) and molecular weight (μ, solid and dashed curves; left y-axis) as a function of pressure P (cgs units) for the structure with $M = 0.3\ M_\odot$, $Z = 0.0006$, $Y = 0.24$ and age = 10 Gyr. The solid and dash dotted curves correspond to EOS+OPAL while dashed and dotted curves are calculated with EOS+SCH (see text).

In Fig. 2 we show the differences in the molecular weight (μ) and adiabatic gradient $\nabla_{\rm ad} = \mathrm{d}\log P/\mathrm{d}\log T$ along the structure of two main sequence models of $M = 0.3\ M_\odot$, $Z = 0.0006$ at the age of 10 Gyr, computed with the two different EOS. The

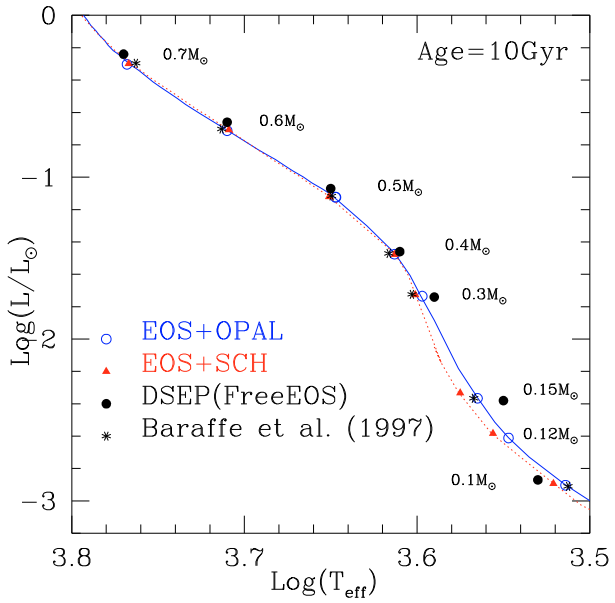

Fig. 3. HR diagram location at 10 Gyr for models with $Z = 0.0006$, the labelled masses are calculated with different EOS tables. Models from the Dartmouth Stellar Evolution Database (full dots) and from Baraffe et al. (1997) (asterisks), with the same metallicity as ours, are also shown for comparison.

differences are more evident in the zone of partially ionization where physical differences of the two treatments (different μ) affect ∇_{ad}. In the EOS+SCH models, the regions in which ∇_{ad} is lower prevail, and the global effect is to produce $T_{\rm eff}$ larger by about 100 K practically at the same luminosity, since the inner structure does not change significantly with the EOS.

The results for different masses are shown in Fig. 3, reporting the HR location of the models at 10 Gyr. The differences are small for $M \geq 0.5\ M_{\odot}$, where the regions of partial ionization do not dominate, and vanish at the lowest masses, because only the EOS+SCH is available for the physical conditions of their interiors.

Based on these results, we may conclude that use of both EOS leads to models with compatible effective temperatures and luminosities. In Fig. 3 we report the location of the models of same chemistry computed by Dotter et al. (2007) for the available masses, with the Dartmouth Stellar Evolution Program (DSEP), using the FreeEOS by Irwin (2004)[4] and otherwise very similar input physics (L and $T_{\rm eff}$'s are taken from their WEB page); for the same masses the models by Baraffe et al. (1997) are also shown. Note that these latter models do not differ significantly from ours both in L and $T_{\rm eff}$, while the models calculated with DSEP at the lowest masses differ, especially in $T_{\rm eff}$, up to ~300 K at 0.15 $M_{\odot}$. This effect can be possibly attributed to the different EOS, but a detailed comparison of models would be required.

3.3. Convection

The ATON code allows us to model turbulent convection by adopting the traditional Mixing Lenght Theory (MLT, Bohm-Vitense 1958) or the "Full Spectrum of Turbulence" (FST) model (Canuto & Mazzitelli 1991; Canuto et al. 1996) which takes into account the full eddies energy distribution (see Canuto & Mazzitelli 1991, for a detailed description of the physical differences between the two models).

While for very low mass stars the description of convection has no influence on the atmospheric structure, this does not hold for those masses in which convection has a substantial degree of overadiabaticity, especially for the stars at the turnoff of GCs. For these models a homogeneous modelling of convection in the atmosphere and the interior is highly recommended. At $T_{\rm eff} > 4000$ K, the grids of models computed by Heiter et al. (2002) by means of NEMO, a modified version of Kurucz's code, are available. These grids are provided both with the MLT model and with the FST model by Canuto et al. (1996). A preliminary version of these latter grids has been used by Montalbán et al. (2001) and will be used in this paper (where possible).

3.4. Atmospheric structure and boundary condition

At $T_{\rm eff} \lesssim 4000$ K in the outermost layers of very low mass stars, radiative absorption is dominated by molecules, and the outcoming flux is very different from the frequency-averaged distribution provided by grey models (Baraffe et al. 1997; Montalban et al. 2000). At larger $T_{\rm eff}$, the atmospheric models become less critical, whereas the $T_{\rm eff}$ itself is heavily influenced by the treatment of overadiabatic convection. For the non-grey models that employ an MLT treatment of convection in the atmosphere with a given $\alpha_{\rm atm}$, not only the $\alpha = l/H_p$ used in the interior computation ($\alpha_{\rm in}$) affects the $T_{\rm eff}$, but also the optical depth at which the match between the atmospheric and the interior integration is made, and also the value of $\alpha_{\rm atm}$ (Montalbán et al. 2004). Montalbán et al. (2001) have shown that the use of the NEMO grids of model atmospheres (Heiter et al. 2002) computed with the FST convection may provide a good match to the interior models computed with the same convection model in the interior, independently of the matching optical depth.

For the above two reasons we use boundary conditions according to the stellar mass based on two different grids of non-grey models of atmosphere[5]. For $M \geq 0.5\ M_{\odot}$ we use Heiter et al. (2002) FST grids and also FST convection in the interior computations, whereas for $M \leq 0.5\ M_{\odot}$ we adopt the NextGen grids by Hauschildt et al. (1999) computed by the PHOENIX code with the MLT treatment of convection and $\alpha_{\rm atm} = l/H_p = 1$. The available grids extend down to $T_{\rm eff} = 800$ K for the [M/H] = −2.0 models, but just down to 2000 K for larger metallicity. For these $M \leq 0.5\ M_{\odot}$ models, we adopt MLT convection also in the interior computation, setting $\alpha_{\rm in} = 2.0$[6]. Since the model atmospheres are computed assuming an ideal gas and Saha-like thermodynamics, they should not be used in the real gas domain where pressure effects are relevant. A relatively small value of the optical depth is chosen for the match between atmosphere and interior. We use $\tau_{\rm ph} = 3(10)$ for $M < (\geq) 0.5\ M_{\odot}$. Notice that the grids of model atmospheres available are computed only for solar scaled mixtures. The lack of suitable model atmospheres for α-enhanced populations forces us to use a grid for the boundary atmospheric conditions with larger [Fe/H] to simulate the α-enhancement, following the procedure adopted

[4] http://freeeos.sourceforge.net/

[5] The same approach has been adopted for pre-main sequence stars in Di Criscienzo et al. (2009).

[6] The choice of the α parameter is less and less critical when decreasing the mass, as the external layers become so dense that convection becomes more and more adiabatic. Nevertheless, we use $\alpha_{\rm in} = 2.0$ to allow for a smooth $T_{\rm eff}$ transition between the upper ($M \geq 0.5\ M_{\odot}$) and lower ($M \leq 0.5\ M_{\odot}$) MS models.

by Baraffe et al. (1997). We use a grid for [Fe/H] = −1.7, obtained through interpolation between the grids for [Fe/H] = −2.0 and −1.5, to compute α-enhanced models with $Z = 0.0002$.

3.5. Transformations to observational plane

In order to compare the models to the photometric data in NGC 6397 we convert luminosity, $T_{\rm eff}$ and surface gravity into absolute magnitudes and colors in the ACS filters. The method most used is to calculate theoretical stellar spectra from atmosphere models and to convolve these synthetic spectra with the filter transmission curves for a photometric system which defines the transmission of light through the filter as a function of wavelength. Uncertainties derive especially from the missing or incorrect absorption features and simplifying physical laws as the assumption of LTE. On the other hand, semiempirical colors and bolometric corrections (e.g. Vandenberg & Clem 2003) have other uncertainties, e.g. they depend on the assumed distance (Dotter et al. 2007).

For the specific case of ACS filters, we use the procedure by Bedin et al. (2005). They computed ACS color indices by using a homogeneous set of ODFNEW model atmospheres and synthetic fluxes computed with the Kurucz ATLAS9 code (Castelli & Kurucz 2003). Grids of magnitudes for different values of [Fe/H], for 3500 K $\leq T_{\rm eff} \leq$ 50 000 K, $0 \leq \log g \leq 5.0$ and microturbolent velocity 2.0 km s^{-1} are provided. Visual bolometric correction BC_V, visual magnitude M_V, and color indices $M_V - M_{ACS}$ are given. The ACS magnitudes were computed by using the WFC/ACS transmission curves by Sirianni et al. (2005), while they adopted the V passband from Bessel (1990). Finally, they assumed that the Vega ACS magnitude would be equal to 0.00 in all passbands.

The bolometric corrections by Bedin et al. (2005) for ACS filters do not extend below $T_{\rm eff}$ = 3500 K. For these low temperatures we can use the values obtained from the synthetic spectra of Hauschildt et al. (1999). In this case the transmission filters of Sirianni et al. (2005) were used as well, and zero point corrections to standard systems are obtained from observed Vega spectra.

Obviously the availability of a unique set of colors-$T_{\rm eff}$ transformations would be highly recommended; but for masses below 0.5 $M_\odot$, we have at least the advantage t use the same bolometric corrections derived from the atmospheric structures used as boundary conditions for the stellar models.

Finally we note that the two sets of correlations match very well in the main sequence, so that no discontinuity arises in our transformed isochrones.

4. Results: solar scaled models

We computed evolutionary tracks for low mass objects ($M \leq 0.8\ M_\odot$) from the pre-main sequence to the red giant branch, or until they reach an age of 20 Gyr. Results are shown here for [M/H] = −1.5 and [M/H] = −2.0, but larger metallicities ([M/H] = −1.00 and −0.50) are available upon request.

In this section we present results for solar scaled mixtures (Grevesse & Sauval 1999, GS1999), [α/Fe] = 0.4 models will be used in Sect. 6 to compare with the data of NGC 6397. Models are extended down to the HBMM when the atmospheric boundary conditions allow for it.

We computed standard evolutionary tracks with an initial helium content close to the Big Bang abundance (that is $Y = 0.24$, Coc et al. 2004) and models with larger helium ($Y = 0.28$, 0.32 and 0.40). From the evolutionary tracks, isochrones are derived for typical ages expected for GCs, from 10 to 14 Gyr.

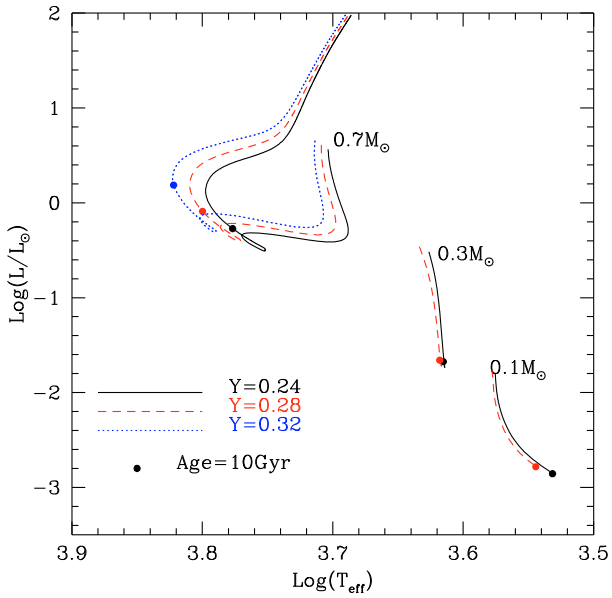

Fig. 4. Evolutionary tracks, starting from the pre-main-sequence, for three different masses with $Z = 0.0006$ and the different value of initial helium.The filled circle labels the position in the HR diagram of the star at age = 10 Gyr. Only for the highest mass the tracks with the all three Y are shown.

Figure 4 compares the HR diagram evolution for three different masses (M = 0.70, 0.30 and 0.10 $M_\odot$) and different Y. Models with a larger helium abundance have larger luminosity and $T_{\rm eff}$ due to the on average greater mean molecular weight μ. This effect is more evident in the stars with a radiative core (shown heare is the M = 0.7 $M_\odot$) than in the completely convective stars like the 0.3 $M_\odot$. The difference increases again in the lowest masses ($\lesssim$0.15 $M_\odot$), where partial degeneracy begins to play a role.

4.1. Mass-luminosity relation

The mass-luminosity relation (MLR) is essential for the comparison with the data, as it enters in the conversion of the (assumed) mass function into the luminosity function (LF).

Any change of slope of the MLR will be reflected in the luminosity function, which is defined as $dN/dL = dN/dM \times dM/dL$. Where the MLR presents an inflection point, the LF has a relative maximum or minimum. As the luminosity decreases along the MS, there are two inflection points, responsible for two main peaks in the LF (see Fig. 7): the first, at $M_{F814W} \sim 6$ mag, is due to the transition between pure MS models and models that suffer the effects of evolution (and are more luminous in the MS due to the hydrogen consumption). Therefore, the corresponding peak in the LF is a function of age, and also as we will see, of Y. After a small range of homologous models, the MLR steepens progressively due to the onset of molecular absorption in the stellar envelope; this produces a gradual increase in the LF. When models become fully convective at ∼0.35 $M_\odot$, the MLR relation begins to flatten again, and the presence of this inflection point results in the large peak at $M_{F814W} \sim 8$ mag, which is present in all the GC LFs (D'Antona 1998) and is shown in Fig. 7.

Finally, at masses $M \sim 0.12\ M_\odot$, the MLR relation flattens even more. This is due to the onset of degeneracy in the core

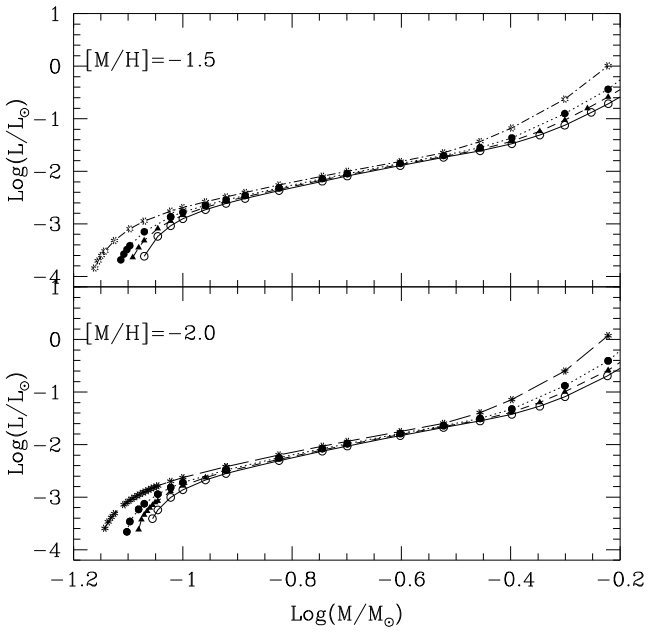

Fig. 5. The MLR for models at 10 Gyr having the labelled value of metallicity and different helium abundance (=0.24-open circles, =0.28-filled triangles, =0.32-filled circles, =0.40-asterisks). In each case the lower masses are the derived HBMM and reported in Table 1.

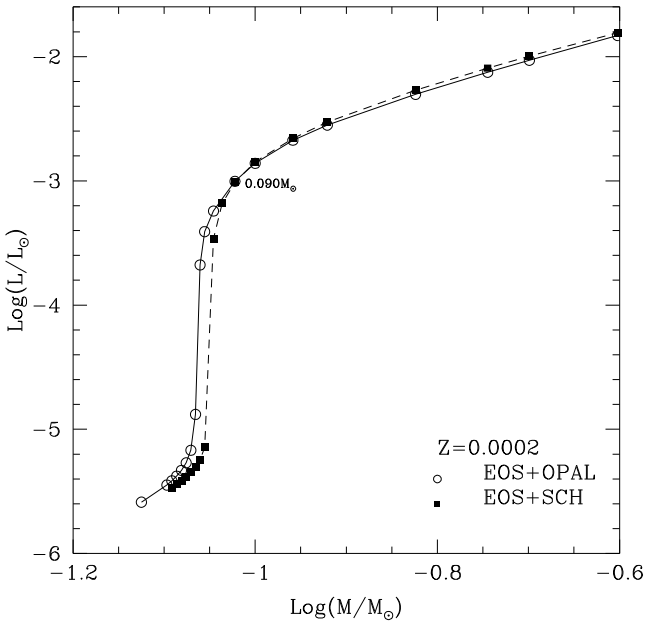

Fig. 6. Comparison at very low masses between the MLR obtained using models computed with different equations of state (see text).

Table 1. Hydrogen burning minimum mass (HBMM) for $Z = 0.0002$ and $Z = 0.0006$, [α/Fe] = 0, and different Y.

	$Y = 0.24$	$Y = 0.28$	$Y = 0.32$	$Y = 0.40$
$Z = 0.0002$	0.088 $M_\odot$	0.083 $M_\odot$	0.079 $M_\odot$	0.072 $M_\odot$
$Z = 0.0006$	0.085 $M_\odot$	0.081 $M_\odot$	0.077 $M_\odot$	0.069 $M_\odot$

of the star (D'Antona 1998), and this subsequent decrease in the LF is dependent on the EOS. The HR diagram does not show the minute features of the MLR derivative, but it shows two "kinks", the first one corresponding to the onset of molecular hydrogen dissociation in the envelope (Copeland et al. 1970) and the second to the onset of degeneracy.

In Fig. 5 we show the dependence of the MLR on the metallicity and helium content at 10 Gyr. Y mostly influences the evolved part of MS and the location of the very low masses, where degeneracy sets in and the second MS kink is located. At the MS end, decreasing the mass, the higher helium models remain more luminous and hotter. These features will affect the low luminosity LF, which will decrease more slowly with decreasing luminosity for larger Y. At the brightest MS luminosities, the larger the Y, the smaller the slope of the MLR of those models that partially burn their hydrogen during a Hubble time with respect to the case of $Y = 0.24$. This is an obvious feature of the evolutionary models: larger Y produces larger MS luminosities and faster MS evolution.

The quantitative results concerning the lowest luminosities will also depend on the EOS, as we can easily understand by comparing the MLR relations obtained using EOS+OPAL and EOS+SCH tables (Fig. 6). For masses larger than 0.1 $M_\odot$ the models using EOS+SCH are slightly more luminous as a consequence of the differences in ∇_{ad}, but the trend is reversed closer to degeneracy. Obviously this variation in the slope of the MLR will produce a different shape in the peak of the LF, and in particular we expect a stronger peak when EOS+SCH are used.

An interesting theoretical feature of the models at the boundary between low mass stars and brown dwarfs is shown in Fig. 6. This figure refers to the $Z = 0.0002$ case, for which an extended atmospheric grid is available. In between the HBMM – the smallest mass that stabilizes in MS, in a configuration in which the total luminosity is provided by the proton−proton (p−p) reactions in the core – and the pure brown dwarfs – that never ignite the p−p chain – there is a small range of masses for which nuclear burning contributes to the stellar luminosity for even several billion years, but in the end these objects finally cool as brown dwarfs. This is a common occurrence in population I (the transition masses defined in D'Antona & Mazzitelli 1985), where the MS merges without discontinuities into the brown dwarf cooling sequences. On the contrary, the MS of the population II has a much sharper drop, because the much smaller opacities put the HBMM at minimum luminosity a factor of about ten higher, so that the transition masses cover a very small mass range. There is then a "luminosity gap" between the end of the MS and the luminosity at which the smaller brown dwarfs are able to slow their cooling down to the typical age of population II stars (10−12 Gyr). Figure 6 translates into possible LF. In Fig. 7 LFs for 10 and 13 Gyr are plotted, assuming a power law MF with an exponent $\alpha = -0.5$. At 13 Gyr, the low mass brown dwarfs should emerge as a small peak at $M_{F814W} \sim 18$, corresponding to near infrared magnitudes of ∼30 at the distance of NGC 6397. The peak is ∼1 mag brighter if the age is 3 Gyr smaller. We regard this prediction as an educated guess on the possibility that the dimmest luminosities regime is populated not only by white dwarfs (Richer et al. 2008) but also by very cool brown dwarfs. However, dynamical models indicate that these objects should be preferentially stripped from the cluster. Since there is a strong difference in these two populations, as the cool white dwarfs would be located at a color $M_{F606W} - M_{F814W} \sim 1-1.2$ mag, while the cool brown dwarfs will not be visible in the $F606W$ band, as they have $M_{F606W} - M_{F814W} \sim 5.5-7$ mag, only future observations with even more capable telescopes should clarify the issue.

Table 2. Descriptions of the chemistry of the models calculated for this work.

Name	Description	Z	[C/Fe]	[N/Fe]	[O/Fe]	Reference
		$Z = 0.0006$				
CNOx1s	Solar-scaled	0.0006	0.00	0.00	0.00	GS1999
CNOx1a	[α/Fe] = 0.40	0.0006	0.00	0.00	0.40	GS1999
		$Z = 0.0002$				
CNOx1s	Solar-scaled	0.0002	0.00	0.00	0.00	GS1999
CNOx1a	[α/Fe] = 0.40	0.0002	0.00	0.00	0.40	GS1999
CNO↑	total(CNO) = 1.6	0.0003	0.00	1.40	0.20	this work

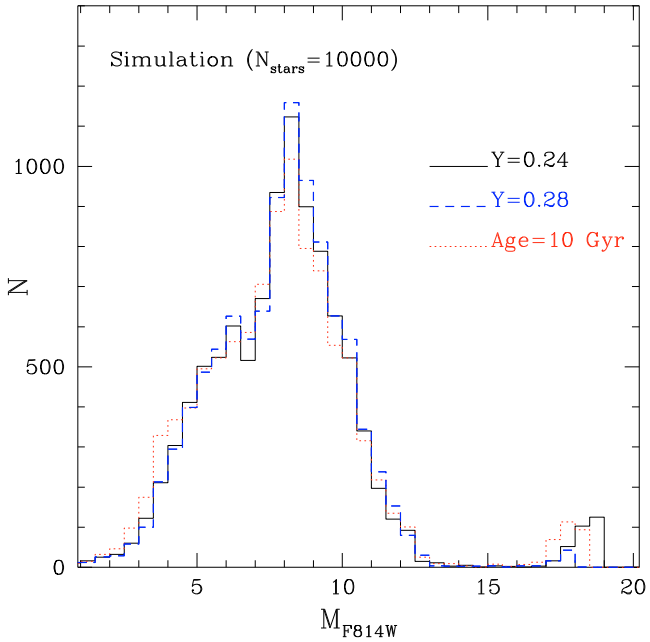

Fig. 7. Theoretically predicted luminosity function for the models at the age = 13 Gyr with $Z = 0.0002$ and two different helium abundances. A power law with the exponent $\alpha = -0.5$ was used as a mass function. The LF at age = 10 and with $Y = 0.24$ isalso shown for comparison.

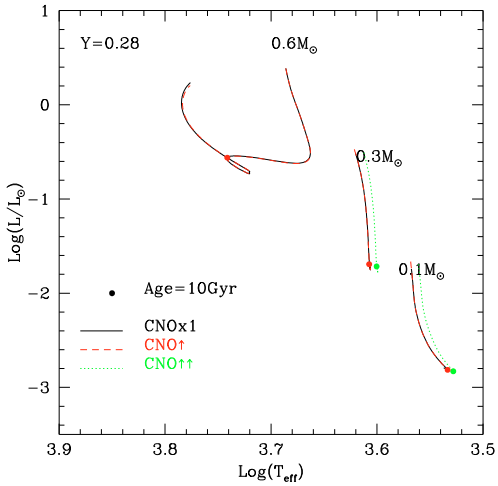

Fig. 8. We show the comparison between the diagram of the standard CNO tracks at different masses(full line) and the "peculiar" ones calculated (dashed and dotted line) with the evolution of the same mass.

5. α-enhanced models, FG and SG populations, CNO enrichment

A comparison with low metallicity cluster stars requires the use of models with α-enhanced mixtures, for which we adopt [α/Fe] = 0.4. As discussed only up to ∼30% of stars of NGC 6397 can belong to the FG, the majority show indeed the Na−O anticorrelation, and many stars have a very high nitrogen content. Therefore we also need models to represent the SG. We will assume that it may differ both in helium content and in total CNO content from the standard FG. A resonable assumption for CNO is that we assume an over-abundance of N by about 1.4 dex and a variation of −0.2 dex for O, leaving carbon unchanged (Bragaglia, private comunication). The total "metallicity" Z in the mass fraction for this CNO-enhanced mixture (CNO↑) is now $Z = 0.0003$. We used the OPAL Web tool to radiative opacities compute on purpose for this mixture. For $T \leq 15\,000$ K we still use the opacities by Ferguson et al. (2005), as lower temperature opacities do not affect the structure of the models we are considering. All models are computed for a helium mass fraction of $Y = 0.24$ and $Y = 0.28$ and are summarized in Table 2.

In general, as discussed in the analysis by Ventura et al. (2009), the largest differences between standard and CNO-enhanced mixtures are found in the ionization zone of the CNO elements, but in this case the differences are very small since the variation is not very significant, and the initial abundances are very small. As a result, pratically no differences are found in effective temperature and luminosity of the models (see Fig. 8).

Another possible hypothesis is that oxygen in the SG is basically similar to the FG value, as most of the Carretta et al. (2009a) measurements for O are only upper limits. In this case, the CNO abundance becomes even larger. We accordingly adopt as boundary conditions the grid [M/H] = −1.5. (CNO↑↑ models, see Table 2). As reported in Fig. 8 the differences in this case are very small as well, but for masses of about 0.3 $M_\odot$ the temperature is a little lower.

6. Comparison with the data of NGC 6397

We analyze both the CMD diagram and the luminosity function simulations.

6.1. Color–magnitude diagram

In Fig. 9 we compare the models with the deep photometry of NGC 6397 by Richer et al. (2008). We plotted the isochrone that allows for the best fit of both the low main sequence and the TO for the labelled value of distance modulus and reddening, with [Fe/H] = −1.99 dex (Carretta et al. 2009c) and [α/Fe] = 0.4 (solid line-red in the electronic version) and with an age of 12 Gyr, which is comparable with the age obtained from the white dwarf cooling sequence of NGC 6397 by Hansen et al. (2007). The distance modulus in the *F814W* photometric band is compatible with the true distance modulus (=12.03 mag) and

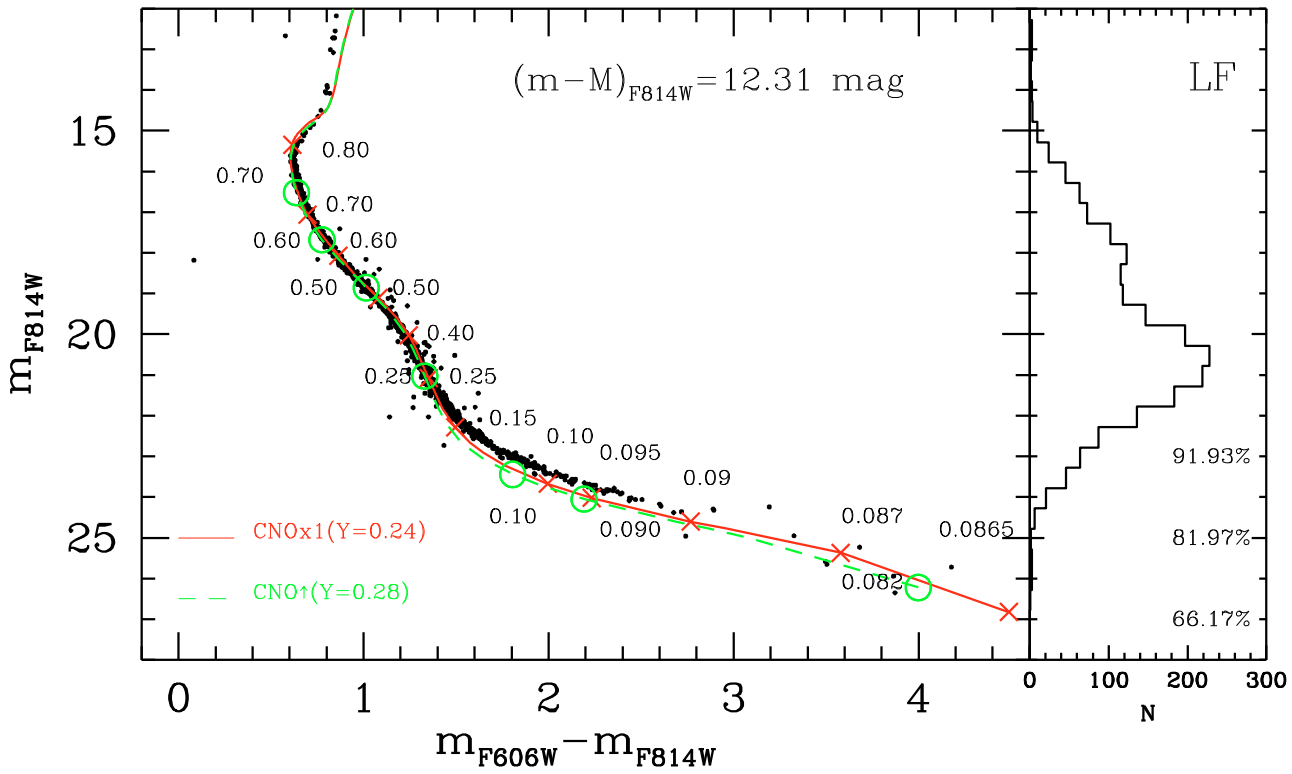

Fig. 9. *Left panel*: main Sequence of NGC 6397 from Richer et al. (2008). Also shown are the best-fit isochrones for FG (red) and SG (green) populations. Numbers indicate stellar masses (up-FG, down-SG) of the same models (crosses-FG, open circle-SG) in $M_{\odot}$ units. *Right panel*: NGC 6397 MS luminosity function from data; for three low luminosities the completeness fraction taken from Table 4 of Richer et al. (2008) is reported.

$E(F606W - F814W)$ (=0.20 mag) reported in literature (see for example Table 3 of Richer et al. 2008).

As already found by Richer et al. (2008), below 0.20 $M_{\odot}$ the isochrone and the data do not match perfectly, but the data appear to terminate at about the magnitude predicted by models. We thus confirm the suggestion of Richer et al. (2008) that they have observed the termination of the hydrogen burning sequence.

In Fig. 9 we also show (dashed line-green in the electronic version) the position of the isochrone obtained with models computed with $Y = 0.28$ and CNO↑ using the same distance modulus and age as used for the FG isochrone. The two isochrones are very similar except around $m_{F814W} = 23$ mag, where they deviate and the FG isochrone is a little brighter. This aspect is important to understand if the tightness of the MS at this interval of magnitude depends on observational error only or is the consequence of the presence of a second generation made of stars with higher helium abundance and CNO enhancement. We select data within three different intervals of half magnitude below the MS turnoff, and rectify their colors by subtracting the color of their best-fit line, as shown in Fig. 10, in the left and medium panels. We do not consider the possible presence of binaries, as Davis et al. (2008) have shown that NGC 6397 has a primordial binary fraction of only ∼1%. The histogram of the color displacements from the best-fit line, shown in the right panels, is fitted with a Gaussian profile with the labelled $\sigma_{\rm obs}$.

In the same panel we report the color displacements for each interval of magnitude for synthetic populations (assuming the distance modulus for NGC 6397 reported in Fig. 9) under the hypothesis that 30% of all stars are primordial (standard helium and CNO abundance), and the remaining 70% are composed by a mixture of SG population with CNO↑ and helium respectively up to Y = YUP = 0.25, 0.26 and 0.28. As expected, the largest difference between σ is obtained in the third interval of magnitude. From the values of dispersion reported we obtain that a SG made of stars with helium dispersion of $\Delta Y = 0.02$ is compatible with the tightness of the MS of NGC 6397.

In the case of the CNO↑↑ models (see Sect. 5) the isochrone calculated for $Y = 0.28$ overlaps exactly on the FG's. In this case the observational spread of MS at low magnitude may suggest an even broader spread of helium between FG and SG.

6.2. Luminosity function

We now compare the observed luminosity function with the theoretical simulations. We use the magnitudes in the *F814W* filter and derive synthetic populations from models at different ages, in the plausible range from 9 to 14 Gyr.

The mass-luminosity relation from our models was discussed in Sect. 4.1; now we discuss the choice of the mass function (MF). We consider this cluster initially as formed by unique population to define a method to compare the theoretical and observational luminosity function. Due to the dynamical evolution of the cluster, the present MF is not the initial one. NGC 6397 has a collapsed core (Djorgovski & King 1986), as it has evolved past the potentially catastrophic phase of core collapse, and is dynamically old. In particular it has been shown that NGC 6397 exhibits mass segregation, which certainly has affected the MF (Hurley et al. 2008). Silvestri et al. (1998) have shown, adopting their own low mass models and those by Baraffe et al. (1997), that the bulk of the MF can be described by a unique power law of the form $dN/dM = k\ M^{\alpha}$ with index $\alpha = -0.5$. Richer et al. (2008) found that $\alpha = -0.13$ gives the highest χ^2 when

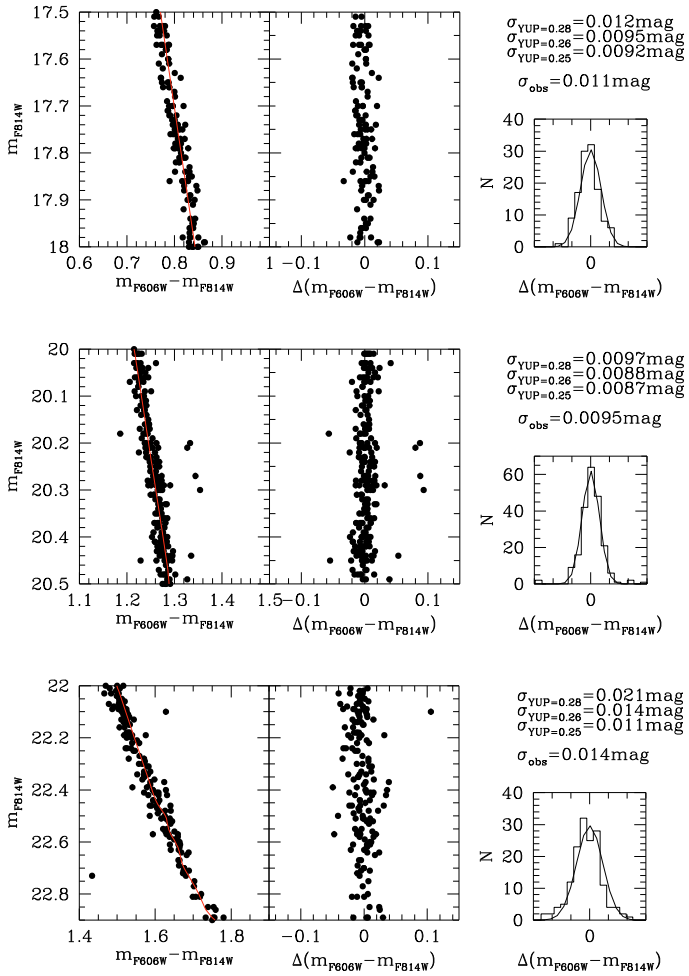

Fig. 10. **a)** In each row a small portion of the MS of NGC 6397 is shown on the far left, while in *the middle panel* the magnitude m_{F814W} is reported versus the color distance from the best-fit line. On *the right panel* we show the histogram of the color displacements, fitted with the best-fit Gaussian curve for the data. We also report the σ of the best-fit Gaussian curve obtained for the synthetic population made up of the 30% of stars belonging to FG and the remaining 70% made of stars of SG with different YUP.

comparing the models with their data of NGC 6397. They found an even better result when a lognormal distribution is used, which has the advantage to truncate the LF at the extreme low mass end, but the disadvantage to introduce a new parameter. A similar result was obtained by De Marchi et al. (2000) who suggested that no single power law distribution is compatible with the MS of NGC 6397; in particular they found that the MF is less steep for $M \leq 0.3\ M_{\odot}$.

We simulate the synthetic populations using a power law MF with two different slopes above (α_H) and below (α_L) a cutoff magnitude of the range of $M_{F814W,\mathrm{cut}} = 8.5{-}10.5$ mag (here we consider a single MF as a particular case with $\alpha_H = \alpha_L$); this cutoff magnitude corresponds to a "cutoff mass" for a chosen distance modulus At a fixed age, MLR gives the magnitudes of each extracted mass according to the chosen MF, which depends on four parameters (α_H, α_L, $M_{F814W,\mathrm{cut}}$ and distance). We simulate photometric errors considering gaussian errors for the magnitudes of each extracted mass to reproduce the width of the upper main sequence. In addition we have taken into consideration the uncertainties in completeness by multiplying the random extractions in a given interval of masses for the completeness fractions given in Table 4 of Richer et al. (2008) which determined with the artificial star test described in Anderson et al. (2008).

We have then used the Kolmogorov-Smirnov test to compare the observed luminosity function of NGC 6397 with the theoretical one, which depends on the MF used to extract masses (α_H, α_L $M_{F814W,\mathrm{cut}}$), as well as on the age and distance modulus. This statistical method has the advantage of being non-parametric, and without making assumptions about the distribution function of the data, it returns the probability that two arrays of data values are drawn from the same distribution. The scalar KS[7] (varying between 0 and 1) gives the significance level of the KS statistic, i.e. the probability with which we can accept the null hypothesis. KS = 1 means that the simulated and observed data follow the same function.

Another great advantage of this statistical method is that the two arrays of data do not need to have the same number of elements; this means that we can build our synthetic populations with a greater number of stars then the actual number of stars from which we derived the observed LF, making the results independent from the random extraction. We have studied the dependence of KS numbers as a function of distance modulus for each of the four free parameters (age, α_H, α_L and $M_{F814W,\mathrm{cut}}$) used to build the synthetic population, and then we have compared the results to choose the best fit parameter. In particular as done by Richer et al. (2008) for their χ^2 method both α_H and α_L were allowed to range from -1 and 1 in 200 steps. We have explored the case of a single MF as a special case in point ($\alpha_H = \alpha_L$). We find that the best combination of power law exponents for higher and lower masses, respectively, are $\alpha_H = -0.7$ and $\alpha_L = -0.1$. The upper panel of Fig. 11, where the variation of KS are shown with the distance modulus for various selected α_H, justifies our choice. We also note that the distance modulus for which we have the higher probability is about the same distance modulus for which we have the best comparison between isochrones and CMD (see Fig. 9), which further confirms the validity of our method. The same result is obtained using models with higher helium abundance. For these values we also report in Fig. 11 KS as a function of distance modulus for different ages (medium panel) and for different cutoff magnitudes (lower panel). In the bottom panel the case of a single power law with an index of -0.7 is also shown (black triangles): we see that a unique power law does not give a good match to the observed LF. Notice however that for higher masses this value is very different from the one obtained by Richer et al. (2008) ($=-0.13$). Still we wish to stress that our result is consistent with their consideration that a lognormal function produces better χ^2 values than the best fitting single power law MF. In fact, when a lognormal function is used one has two adjustable parameters, as in our case. Concerning the age, as shown in the medium panel of Fig. 11, the best agreement with observations is obtained for an age of 14–13 Gyr, but if we also consider the best distance moduli and take into account the CMD we can choose 12 Gyr together with $M_{F814W,\mathrm{cut}} = 9.5$ mag, corresponding to $M \sim 0.18\ M_{\odot}$[8].

In Fig. 12 we report the NGC 6397 MS LF compared with the best fitting double power law mass functions. The overall agreement is satisfactory. Only at $M_{F814} \geq 12$ mag ($\sim M = 0.090\ M_{\odot}$), are the observed stars fewer then predicted; this could mean that the MF is even flatter at these lowest masses due to more effective evaporation, but it may also be due to some

[7] We use the `kstwo` algorithm from "Numerical Recipes", 3nd edn.

[8] This value is much lower then the mass ($\sim 0.3\ M_{\odot}$) found by De Marchi et al. (2000).

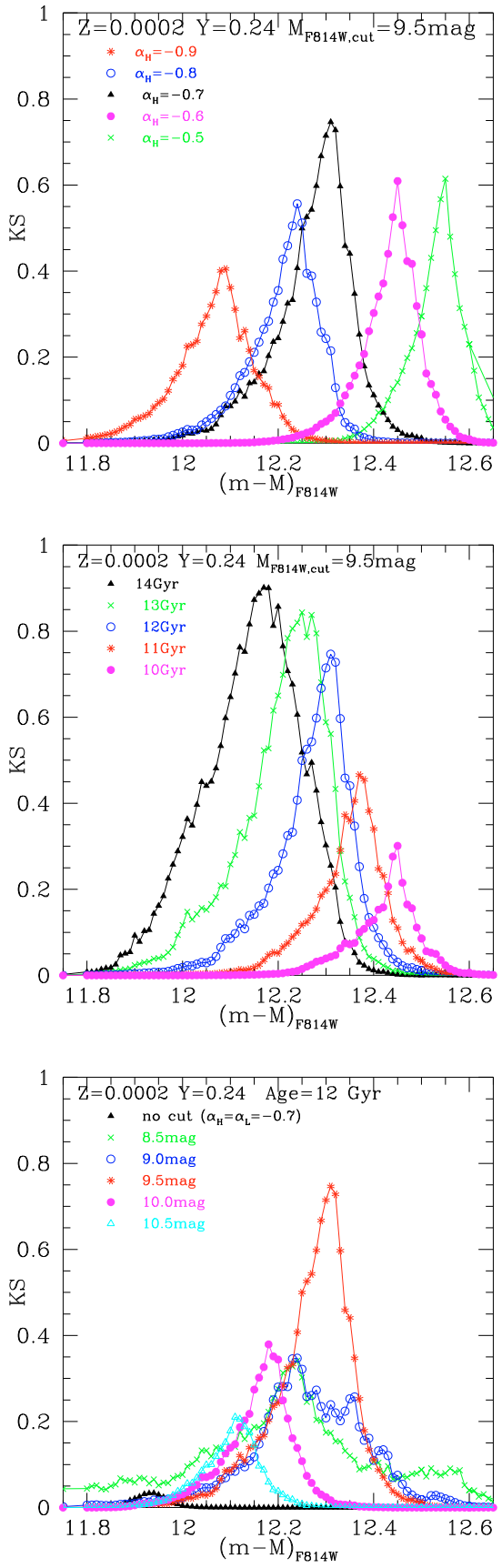

Fig. 11. Distribution of KS with distance modulus for the labelled value of Z and Y and for different α_H ((*upper-panel*)), different ages (*medium-panel*) and $M_{F814W,\mathrm{cut}}$ (*down-panel*) (see text). In all cases a double power law was used with $\alpha_L = -0.1$. In *the medium and down panels* $\alpha_H = -0.7$ as inferred by *the upper panel* is used.

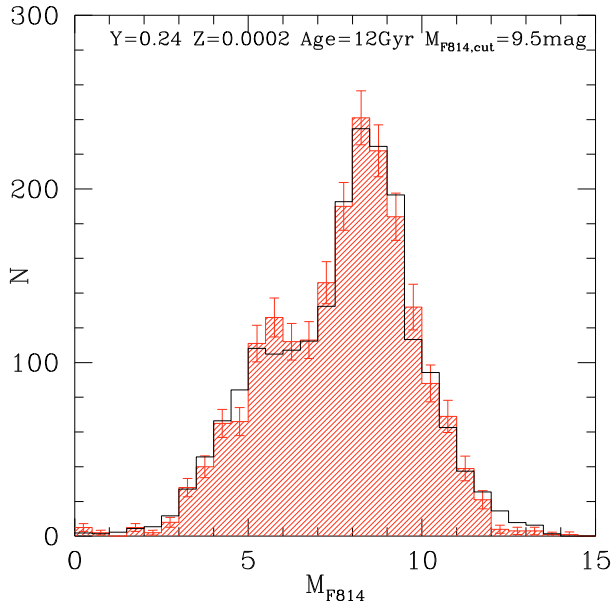

Fig. 12. Comparison between observed and calculated distribution of MS stars of NGC 6397 for the labelled values of the parameters. The power law used is the same as the one of Fig. 11. The error bars take into account the Poisson's error and incompleteness corrections.

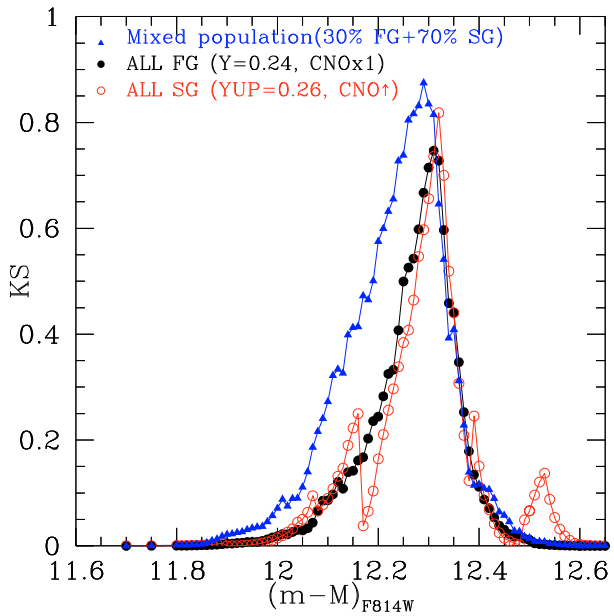

Fig. 13. Distribution of KS with distance modulus for different synthetic populations.

deficiency in the models. In Fig. 13 we also show the distribution of KS in the case that 30% of the stars belong to FG (Y = 0.24 and CNOx1a) and 70% to the SG (YUP = 0.26 and CNO↑), which gives the best match of the width of the MS (see Fig. 10) and in the case where all stars belong to SG. The conclusion is that as comparable KS and reliable distance moduli are obtained in all cases, that is from the width of the MS as well as from the luminosity function, we cannot exclude that the cluster contains either a mixture of stars with different helium, or a single helium abundance for all stars.

7. Conclusions

We have computed new models for the main sequence down to the hydrogen burning minimum mass, adopting two different versions of an updated equation of state and made simulations of the luminosity functions for different choices of the mass function and the initial helium content. The results are compared with the recent observations of the MS of NGC 6397 by Richer et al. (2008). Using a Kolmogorov-Smirnov test to compare observed and simulated LF we found that a double power law for the mass function reproduces the observed luminosity function well in the *F814W* photometric band. However, both the models for a simple or a mixed population according the spectroscopic data provide a good fit of LF. A stronger result is obtained from the analysis of the width of MS from which we find that in any case any helium variations must be confined within $\Delta Y = 0.02$ in the case of CNO overabundance predicted by a mixing between 50% of pristine gas and 50% of gas ejected by 5 $M_{\odot}$ AGB stars as suggested by Ventura & D'Antona (2009). Instead we find that a broader spread ($0.02 \leq \Delta Y \leq 0.04$) in helium between the primordial and intermediate generation is compatible with the width of the main sequence when CNO↑↑ models are considered.

The complete sets of isochrones transformed for the ACS filters *F814W* and *F606W*, calculated for this work, are available upon request to the authors and will be soon inserted in site http://www.mporzio.astro.it/%7Etsa/

Acknowledgements. We thank S. Cassisi for providing the color-$T_{\rm eff}$ transformations and J. Anderson, A. Bragaglia, A. Dotter, A. Milone and H. Richer and G. De Marchi for useful discussions. Financial support for this study was provided by MIUR under the PRIN project "Asteroseismology: a necessary tool for the advancement in the study of stellar structure, dynamics and evolution", P.I. L. Paternó and by the PRIN MIUR 2007 "Multiple stellar populations in globular clusters: census, characterization and origin".

References

Anderson, J., King, I., Richer, H. B., et al. 2008, AJ, 125, 2114
Alexander, D. R., Brocato, E., Cassisi, S., et al. 1997, A&Am, 317, 90
Angulo, C., Arnould, M., Rayet, M., et al. 1999, NuPhA., 656, 3A
Baraffe, I., Chabrier, G., Allard, F., & Hauschildt, P. H. 1997, A&A, 327, 1054
Bedin, L. R., Cassisi, S., Castelli, F., et al. 2005, MNRAS, 357, 1038
Bessel, M. 1990, PASP, 102, 1181
Bonifacio, P., Pasquini, L., Spite, F., et al. 2002, A&A, 390, 91
Caloi, V., & D'Antona, F. 2005, A&A, 121, 95
Canuto, V. M., & Mazzitelli, I. 1991, AJ, 370, 295
Canuto, V. M., Goldman, I., & Mazzitelli, I. 1996, ApJ, 473, 550
Cassisi, S., Castellani, V., Ciarcelluti, P., Piotto, G., & Zoccali, M. 2000, MNRAS, 315, 679
Cassisi, S., Potekhin, A. Y., Pietrinferni, A., Catelan, M., & Salaris, M. 2007, ApJ, 661, 1094C
Carretta, E., Bragaglia, A., & Cacciari, C. 2004, ApJ, 610, L25
Carretta, E., Gratton, R. G., Lucatello, S., Bragaglia, A., & Bonifacio, P. 2005, A&A, 433, 597
Carretta, E., Bragaglia, A., Gratton, R. G., et al. 2006, A&A, 450, 523
Carretta, E., Bragaglia, A., Gratton, R. G., et al. 2009a, A&A, 505, 117
Carretta, E., Bragaglia, A., Gratton, R. G., & Lucatello, S. 2009b, A&A, 505, 539
Carretta, E., Bragaglia, A., Gratton, R., D'Orazi, V., & Lucatello, S. 2009c, A&A, 508, 695
Castelli, F., & Kurucz, R. L. 2003, in Modelling of Stellar Atmospheres, ed. N. Piskunov et al., IAU Symp. 210, A20 [arXiv:astro-ph/0405087]
Catelan, M., Borissova, J., Sweigart, A. V., & Spassova, N. 1998, ApJ, 494, 265
Coc, A., Vangioni-Flam, E., Descouvemont, P., Adahchour, A., & Angulo, C. 2004, ApJ, 600, 544
Copeland, H., Jensen, J. O., & Jorgensen, H. 1970, A&A, 5, 12
Chabrier, G., & Baraffe, I. 1997, A&A, 1997
Davis, D. S., Richer, H. B., Anderson, J., et al. 2008, AJ, 135, 2155D
D'Antona, F. 1987, ApJ, 320, 653
D'Antona, F. 1998, The Stellar Initial Mass Function, 38th Herstmonceux Conference, 142, 157
D'Antona, F., & Caloi, V. 2004, 611, 871
D'Antona, F., & Caloi, V. 2008, MNRAS, 390, 693
D'Antona, F., & Mazzitelli, I. 1985, ApJ, 296, 502D
D'Antona, F., Caloi, V., Montalbán, J., Ventura, P., & Gratton, R. 2002, A&A, 395, 69
Decressin, T., Meynet, G., Charbonnel, C., Prantzos, N., & Ekström, S. 2007a, A&A, 464, 1029
De Marchi, G., Paresce, F., & Pulone, L. 2000, ApJ, 530, 342
de Mink, S. E., Pols, O. R., Langer, N. & Izzard, R. G. 2009, A&A, 507, L1
D'Ercole, A., Vesperini, E., D'Antona, F., McMillan, S. L. W., & Recchi, S. 2008, MNRAS, 391, 825
Di Criscienzo, M., Ventura, P., & D'Antona, F. 2009, A&A, 496, 223
Djorgovski, S., & King, I. R. 1986, ApJ, 305, L61
Dotter, A. 2007, Ph.D. Thesis
Dotter, A., Chaboyer, B., Jevremovic, D., et al. 2007, AJ, 134, 376
Ferguson, J. W., Alexander, D. R., Allard, F., et al. 2005, ApJ, 623, 585
Fontaine, G., Graboske, H. C., Jr., & van Horn, H. M. 1977, ApJS, 35, 293
Gratton, R. G., Bonifacio, P., Bragaglia, A., et al. 2001, A&A, 369, 87
Gratton, R. G., Bragaglia, A., Carretta, E., et al. 2003, A&A, 408, 529G
Grevesse, N., & Sauval, A. J. 1999, A&A, 347, 348G
Hauschildt, P. H., Allard, F., & Baron, E. 1999, ApJ, 512, 377
Heiter, U., Kupka, F., van't Veer-Menneret, C., et al. 2002, A&A, 392, 619
Hansen, B., Anderson, J., Brewer, J., et al. 2007, ApJ, 671, 380
Hurley, R. J., Shara, M. M., Richer, H. B., et al. 2008, AJ, 135, 2129
Iglesias, C. A., & Rogers, F. J. 1996, ApJ, 464, 943
Johnson, J. A., & Bolte, M. 1998, AJ, 115, 693
King, I. R., Anderson, J., Cool, A. M., & Piotto, G. 1998, ApJ, 492, L37
Korn, A. J., Grundahl, F., Richard, O., et al. 2007, ApJ, 671, 402
Lee, Y.-W., Demarque, P., & Zinn, R. 1994, ApJ, 423, 248
Lind, K., Primas, F., Charbonnel, C., Grundahl, F., & Asplund, M. 2009, A&A, 503, 545L
Kroupa, P. 2002, Science, 295, 82
Kroupa, P., Tout, C. A., & Gilmore, G. 1993, MNRAS, 262, 545
Magni, G., & Mazzitelli, I. 1979, A&A, 72, 134
Milone, A. P., Bedin, L. R., Piotto, G., et al. 2008, ApJ, 673, 241
Montalban, J., D'Antona, F., & Mazzitelli, I. 2000, A&A, 360, 935
Montalbán, J., Kupka, F., D'Antona, F., & Schmidt, W. 2001, A&A, 370, 982
Montalbán, J., D'Antona, F., Kupka, F., & Heiter, U. 2004, A&A, 416, 1081
Paresce, F., De Marchi, G., & Romaniello, M. 1995, ApJ, 440, 216
Pasquini, L., Ecuvillon, A., Bonifacio, P., & Wolff, B. 2008, A&A, 489, 315
Piotto, G., et al. 2007, ApJ, 661, L53
Potekhin, A. Y., Baiko, D. A., Haensel, P., & Yakovlev, D. G. 1999, A&A, 346, 345P
Pumo, M. L., D'Antona, F., & Ventura, P. 2008, ApJ, 672, L25
Ramírez, S. V., & Cohen, J. G. 2002, AJ, 123, 3277
Rey, S. C., Yoon, S. J., Lee, Y. W., Chaboyer, B., & Sarajedini, A. 2001, AJ, 122, 3219
Richer, H. B., Anderson, J., Brewer, J., et al. 2006, Science, 313, 936
Richer, H. B., Dotter, A., Hurley, J., et al. 2008, AJ, 135, 2141
Rogers, F. J., Swenson, F. J., & Iglesias, C. A. 1996, ApJ, 456, 902
Sarajedini, A., Bedin, L. R., Chaboyer, B., et al. 2007, AJ, 133, 1658
Saumon, D., Chabrier, G., & van Horn, H. M. 1995, ApJS, 99, 713
Silvestri, F., Ventura, P., D'Antona, F., & Mazzitelli, I. 1998, A&A, 334, 953
Sirianni, M., et al. 2005, PASP, 117, 1049
Stolzmann W., & Blöcker, T. 2000, A&A, 361, 1152
Vandenberg, D. A., & Clem, J. L. 2003, AJ, 126, 778
Ventura, P., & D'Antona, F. 2009, A&A, 499, 835
Ventura, P., D'Antona, F., Mazzitelli, I., & Gratton, R. 2001, ApJ, 550, L65
Ventura, P., D'Antona, F., & Mazzitelli, I. 2007, Ap&SS, 420
Ventura, P., Caloi, V., D'Antona, F., et al. 2009, MNRAS, 399, 934